

Singlet–Triplet States Interaction Regions in DNA/RNA Nucleobase Hypersurfaces

Remedios González-Luque, Teresa Climent, Israel González-Ramírez,
Manuela Merchán, and Luis Serrano-Andrés*

*Instituto de Ciencia Molecular, Universitat de València, Apartado 22085,
ES-46071 Valencia, Spain*

Received March 26, 2010

Abstract: The present study provides new insight into the intrinsic mechanisms for the population of the triplet manifold in DNA nucleobases by determining, at the multiconfigurational CASSCF/CASPT2 level, the singlet–triplet states crossing regions and the main decay paths for their lowest singlet and triplet states after near-UV irradiation. The studied singlet–triplet interacting regions are accessible along the minimum energy path of the initially populated singlet bright $^1\pi\pi^*$ state. In particular, all five natural DNA/RNA nucleobases have, at the end of the main minimum energy path and near a conical intersection of the ground and $^1\pi\pi^*$ states, a low-energy, easily accessible, singlet–triplet crossing region directly connecting the lowest singlet and triplet $\pi\pi^*$ excited states. Adenine, thymine, and uracil display additional higher-energy crossing regions related to the presence of low-lying singlet and a triplet $n\pi^*$ state. These funnels are absent in guanine and cytosine, which have the bright $^1\pi\pi^*$ state lower in energy and less accessible $n\pi^*$ states. Knowledge of the location and accessibility of these regions, in which the singlet–triplet interaction is related to large spin–orbit coupling elements, may help to understand experimental evidence such as the wavelength dependence measured for the triplet formation quantum yield in nucleobases and the prevalence of adenine and thymine components in the phosphorescence spectra of DNA.

1. Introduction

Phosphorescence spectra of DNA at low temperatures have been established as consisting of two basic components which originate mainly from thymine and, to a lesser extent, from adenine.^{1–3} Although triplet state formation and phosphorescence data of individual nucleobases and different derivatives in several media and conditions have been reported and reviewed,^{4–7} including recent studies employing external photosensitizers,^{8–10} the specifics of the intrinsic population mechanism of the triplet manifold in each of the nucleobases has not been understood so far. The different fates of their triplet states, explaining, for instance, the prevalence of two of the bases in the phosphorescence spectra of DNA, the absence of triplet guanine signals, or the triplet state involvement in the fast relaxation processes of nucleobases,

in particular for thymine,¹¹ have still to be elucidated. Triplet states of molecular systems are frequent intermediates in important photoinduced reactions. Both their usual biradical character and relatively long lifetimes make them reactive species prone to interacting with other compounds.¹² Triplet states of DNA/RNA purine and pyrimidine nucleobases are not an exception, and they have been determined to participate in UV-promoted photoreactions as the formation of phototherapeutic nucleobase-pharmakon adducts¹³ or the photodimerization of pyrimidine nucleobases, considered to be the most frequent genetic lesion taking place after UV-light irradiation.^{7,14–16} Since most of the recent attention has been focused on the rapid dynamics of the initially populated singlet states of DNA/RNA nucleobases,^{17–22} their intersystem crossing (ISC) mechanisms and triplet states' decay processes are only now starting to be analyzed.^{23–26} The present study aims to present a unified scheme, based on quantum chemical grounds, for the description of the main

* Corresponding author fax: (+34) 96-3544427, e-mail: Luis.Serrano@uv.es.

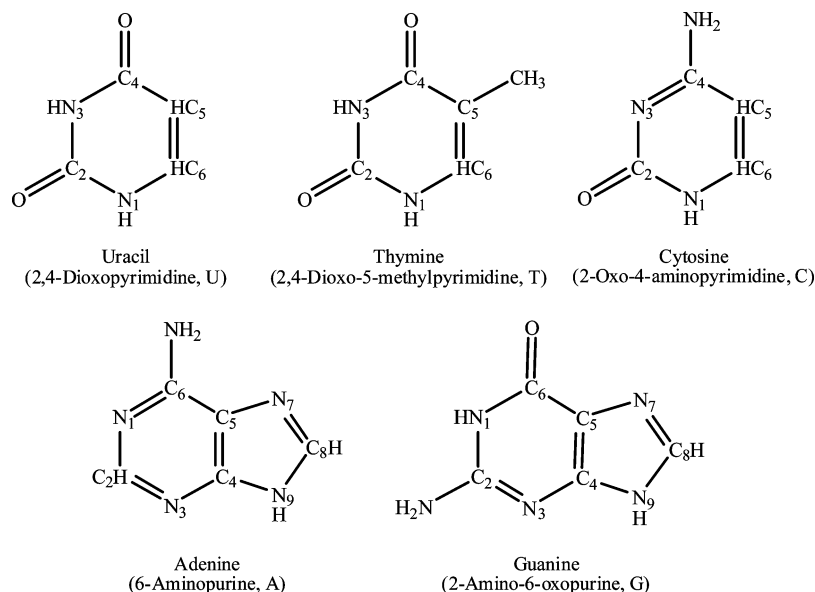


Figure 1. Structure, labeling, common name, IUPAC name, and acronym used for the five natural DNA/RNA nucleobases.

decay pathways for the singlet and triplet states of the five natural DNA/RNA nucleobases, thymine (T), uracil (U), cytosine (C), adenine (A), and guanine (G) (see Figure 1), locating the singlet–triplet crossing regions and computing the related spin–orbit coupling terms in order to provide insight into the intrinsic mechanisms of triplet state population in these molecules and to help rationalize the observed experimental data.

The triplet state population may proceed via endogenous or exogenous photosensitization from other triplet species or by efficient intersystem crossing (ISC) from the initially excited singlet state. There is an essential consensus that efficient radiationless transitions among states of the same multiplicity leading to internal conversion (IC) take place in the close vicinity of conical intersection (CI) regions and that the probability for the decay and the IC rates relate to the size of the nonadiabatic coupling matrix elements between the states.^{27–29} The situation is more complex for the computation of ISC rates. In this case, the efficiency of the interaction between states of different multiplicities, for instance, singlet–triplet, seems to be reasonably well described by the Fermi Golden Rule, which relates the strength of the interaction to the extent of the vibronic spin–orbit coupling (SOC) factors and the Franck–Condon (FC) weighted density of states.²⁷ Recent studies of Marian and co-workers^{26,30,31} have proved that the efficiency of an ISC process relies on a subtle balance of effects, including an enlarged density of vibrational states and a proper overlap of vibrational wave functions which, in turn, enhance the vibronic SOC effects. The decrease of the energy gap between singlet and triplet states, and in particular the presence of singlet–triplet degeneracies, crossing regions, especially when related to the existence of low-energy out of plane vibrational modes, is a good indication of a high density of states, and it is therefore conceivable that singlet–triplet crossings play an important role for increased ISC population transfer rates.¹² This relevance is well-known in the emerging field of multistate reactivity,^{27,32,33} in which the presence of singlet–triplet crossings and the occurrence

of corresponding ISC processes in the vicinity of the ground-state transition state regions become crucial for the enhancement of the reaction rates.³⁴ As they compete with generally faster internal conversion processes, intersystem crossings or spin crossovers can also be expected to be more efficient in energy trapping regions, for instance, near singlet states minima or sloped singlet–singlet conical intersections.^{35,36} Full reaction dynamics calculations including in a balanced and accurate way nonadiabatic and spin–orbit coupling effects for polyatomic systems like those considered here have not been performed yet. Until those studies are available, calculations of ISC rates in which the vibronic spin–orbit and overlap coupling effects are considered give the best information about the efficiency of the ISC process.^{26,30} Our goal in the present research is to determine the presence and accessibility of the singlet–triplet degeneracy regions in natural nucleobases along the main singlet decay pathways and provide hints of their relevance for ISC by computing also electronic SOC terms.

The strategy employed here starts by obtaining the minimum energy paths (MEPs) leading from the primary step of the photochemical process after UV light absorption in DNA nucleobases, being basically the population of the spectroscopically bright singlet excited state, here always the so-called $^1(\pi\pi^* L_a)$ state, toward the singlet–triplet degeneracy regions and finally the lowest-energy and reactive triplet excited state $^3(\pi\pi^* L_a)$, and calculating electronic SOC terms between relevant states.

Recent quantum-chemical *ab initio* CASPT2 studies have provided a unified model for the rapid internal conversion (IC) of the singlet excited DNA/RNA nucleobases manifold^{18,20,29,37–46} that allowed a proper rationalization of the experimental findings.^{17,47} The observed ultrafast decay component in all natural nucleobases, both in the gas phase and in solution, can be interpreted in terms of the barrierless character of the minimum energy path (MEP) associated with the lowest singlet state of the $\pi\pi^*$ type, $^1(\pi\pi^* L_a)$, toward a conical intersection (CI) with the ground state, $(gs/\pi\pi^*)_{CI}$. Secondary decay paths involving the lowest $^1n\pi^*$ state and

even a higher $^1\pi\pi^*$ state have been also identified.^{20,23,29,38–41} Within the context of the photochemical reaction path approach⁴⁸ and the current theoretical paradigm for nonadiabatic photochemistry,^{28,29} it is possible to analyze how the lowest triplet state can be reached efficiently by finding the singlet–triplet crossing (STC) regions more easily accessed from the FC MEP on the $^1(\pi\pi^* L_a)$ state, which represents the major deactivation path responsible of the rapid IC process detected in the molecule. Further studies combining the calculation of ISC rates and wave packet evolution will have to determine how efficient actually are our proposed channels. The obtained results suggest that enhancements in the population yield of the lowest triplet state of the natural DNA/RNA nucleobases can be related to the presence in three of them, T, U, and A, of more ISC channels along the singlet state MEP, in particular those related with low-lying singlet and triplet $n\pi^*$ states that act as intermediate population switchers, unlike what occurs in C and G. The obtained scheme may help to understand how the intrinsic population of the lowest triplet state can take place in vacuo for all the nucleobases, why T and A triplet states seem to prevail on the DNA phosphorescence spectrum and can be expected to have a larger quantum yield of formation (ϕ_{ISC}) than the other nucleobases, and what the molecular basis is for the detected wavelength dependence of ϕ_{ISC} .⁷ Since the calculations have been performed in vacuo, without the explicit consideration of solvent effects, the answer provided here can be regarded as a characteristic molecular property of the nucleobases, which might be expected to be somewhat disturbed by the specific environment in solution, in a solid, in vitro, or in vivo. The presence of the same ultrafast decays has been, however, identified in strands of oligonucleotides in solution,⁴⁹ probably related with the channels of the monomers in relatively unstacked nucleobases.⁵⁰

II. Methods and Computational Details

The present calculations include CASSCF geometry optimizations, MEPs, CIs, and STC searches, followed by multiconfigurational perturbation theory, CASPT2, calculations at the optimized geometries. SOC terms and transition dipole moments (TDM) have also been computed. Radiative lifetimes have been estimated by using the Strickler–Berg relationship,⁵¹ as explained elsewhere,⁵² although their applicability is restricted to cases where radiative deactivation predominates. Their magnitude, otherwise, is only indicative of the prospective emissive characteristics of the state related with the TDM values. For the sake of consistency with previous calculations on the singlet states of the systems, the same one-electron basis sets and active spaces were employed. For the pyrimidine T, U, and C and purine A and G nucleobases, basis sets of the ANO-S type contracted to C,N,O[3s2p1d]/H[2s1p] and 6-31G(d,p) were used, respectively. The final results can be described as CASPT2-(14,10) for T, U, and C, involving an active space of 14 electrons distributed in 10 orbitals, with all valence $\pi\pi^*$ and lone-pair orbitals, and CASPT2(14,12) for A and G, which include all $\pi\pi^*$ orbitals except those related to the deepest canonical orbital plus two lone-pair orbitals. Other active spaces were employed in the optimization procedures,

Table 1. Computed Properties for the Low-Lying Singlet and Triplet Excited States of Adenine

State	vertical transition (eV)		band origin (T _e , eV)		τ_{rad}^b
	CASSCF	CASPT2 ^a	CASSCF	CASPT2	
$^1(n\pi^*)$	5.95	4.96 (0.004)	4.88	4.52	334 ns
$^1(L_b \pi\pi^*)$	5.56	5.16 (0.004)	4.92	4.83	251 ns
$^1(L_a \pi\pi^*)^c$	7.03	5.35 (0.175)			
$^3(L_a \pi\pi^*)$	3.77	4.00	3.52	3.36 ^d	359 ms
$^3(n\pi^*)$	5.38	4.91	4.84	4.41	
$^3(\pi\pi^*)$	5.07	4.95			

^a Oscillator strengths within parentheses. ^b Computed using the Strickler–Berg approximation. See SI. ^c Geometry optimization leads directly to a conical intersection with the ground state, (gs/ $\pi\pi^*$)CI, at 4.0 eV. See refs 29 and 38. ^d Phosphorescence band origin and maximum in solution/glasses: 3.43 and 3.05 eV, respectively. See refs 58 and 59.

following a strategy which was proved successful previously. More detailed technical aspects of the calculations can be found in our previous papers^{23–25,37–39} and in the Supporting Information (SI). All the reported calculations used the quantum-chemical methods implemented in the MOLCAS 7 package.^{53,54}

III. Results and Discussion

The research effort in our group has been focused in recent years on the main singlet decay channels involving DNA/RNA nucleobases as well as several derivatives.^{18,20,37–39} In addition, studies were reported on the lowest triplet population mechanisms of the pyrimidine nucleobases thymine,^{24,26} uracil,^{25,26} and cytosine.²³ Other recent theoretical studies on the vertical and adiabatic energies of the nucleobases' triplet states have also been reported.^{55,56} In the present paper, we outline a unified scheme describing prospective population paths of the triplet manifold in all five natural DNA/RNA nucleobases T, U, C, A, and G, in order to obtain an overall model able to explain the common and the distinct behavior of the systems. Fully new results on the triplet states of the purine nucleobases A and G shall be presented, whereas our previous studies on T and U and new complementary calculations on C will be used and commented upon. The following subsections describe the results for each of the nucleobases. The most relevant conclusions are summarized in the last section.

A. Population of the Triplet Manifold in Adenine.

Table 1 compiles vertical transitions, band origins, oscillator strengths, and radiative lifetimes computed for the transitions to the singlet and triplet states of adenine at the CASSCF and CASPT2 levels of theory. Unless indicated, CASPT2 results will be used in the discussion. Both at the FC region and adiabatically, the lowest-lying singlet excited state is of the $n\pi^*$ ($n_N\pi^*$) type, whereas the one carrying the largest intensity for the related transition, and therefore getting initially most of the population at low energies almost up to 6.0 eV, is the $^1(\pi\pi^*)$ HOMO (H) \rightarrow LUMO (L) (hereafter L_a) singlet excited state at 5.35 eV. The ultrafast nonradiative decay undergone by adenine in the femtosecond range^{17,47} can be rationalized by the barrierless character of the path on this state leading from the FC region toward a CI seam with the ground state, (gs/ $^1\pi\pi^*$)CI,^{29,38,41,43,57} and it is shown also here in Figure 2. Unlike simple geometry optimizations,

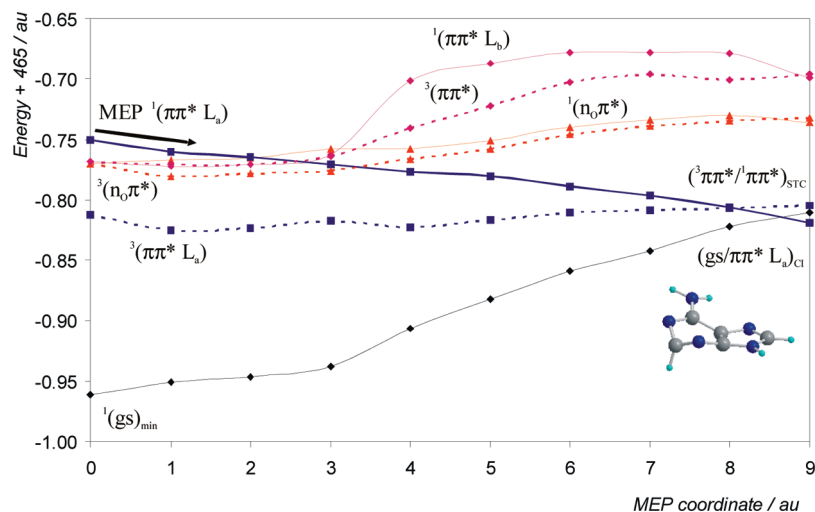


Figure 2. Evolution of the ground and lowest singlet and triplet excited states for adenine from the FC geometry along the $^1(\pi\pi^* L_a)$ MEP.

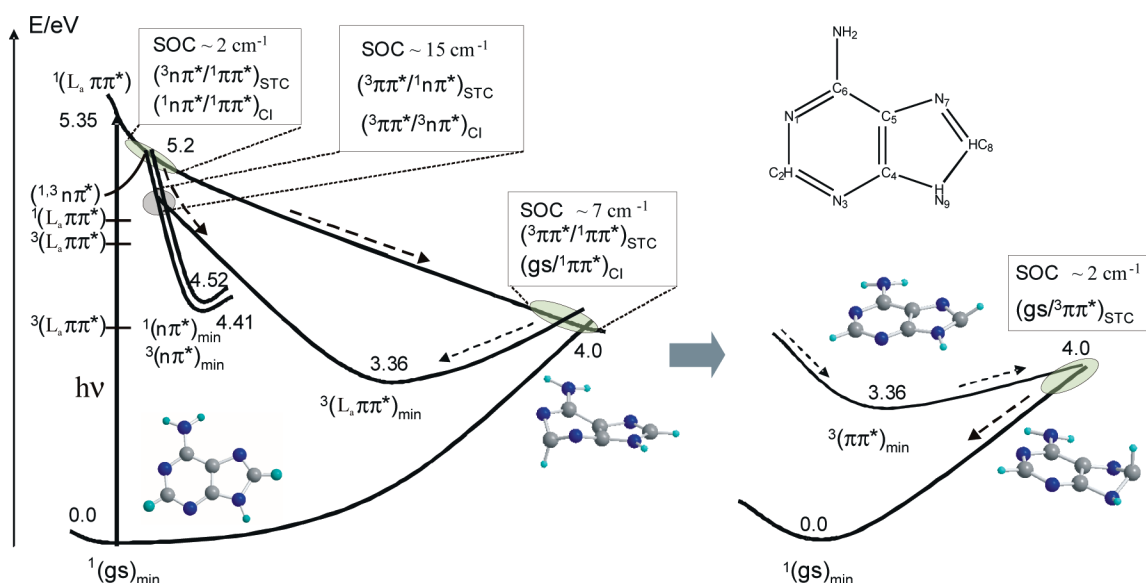


Figure 3. Scheme, based on CASPT2 results, of the photochemistry of adenine focused on the population of the lowest-energy triplet state. Unless otherwise stated, $^1\pi\pi^*$ represents the $^1L_a \pi\pi^*$ state.

the use of the MEP technique guarantees the absence of energy barriers along the lowest-energy path. The structure of the CI at the end of the MEP can be characterized as methanamine-like, involving combined stretching and twisting of the $C_2=N_3$ bond (analogous to a ethene-like CI).^{37–39,60} The presence of an accessible CI explains also the low fluorescence quantum yield ($\sim\phi_F = 10^{-4}$) detected for adenine with a band origin near 4.4 eV in water.¹⁷ This weak emission can be related to the presence of a more polar 7H isomer in solution.^{29,38} A nonfluorescent $^1(n\pi^*)$ minimum is found at 4.52 eV (see Table 1) with a minor contribution to the emissive properties. Similar vertical and adiabatic energy values have been found at other levels of theory.^{21,40,41,43–45,61}

Triplet $\pi\pi^*$ -type states typically lie much lower in energy (here, the lowest one is placed near 1.3 eV) than their singlet counterparts, unlike for $n\pi^*$ -type states, in which a small exchange integral term leads the triplet to be just slightly below the corresponding singlet state. In adenine, for instance, the lowest-energy $^3(n\pi^*)$ state lies, both vertically

and adiabatically, less than 0.1 eV below its singlet analogous state. The consequences for the triplet photophysics of the system are important. Direct singlet $^1(\pi\pi^*)$ –triplet $^3(\pi\pi^*)$ energy transfer seems unlikely in the FC region, where the molecule is almost planar, because of both the large energy gap and low electronic SOC terms ($<0.1 \text{ cm}^{-1}$). The presence of two almost degenerate singlet and triplet $n\pi^*$ -type states at the ground-state geometry can be, however, of high relevance. Along the main decay pathway on S_1 , $^1(\pi\pi^* L_a)$, the state becomes degenerate with different triplet states. As it can be seen in Figures 2 and 3, along the $^1(\pi\pi^* L_a)$ state MEP, two singlet–triplet crossings are described: one at 5.2 eV with the $^3(n\pi^*)$ triplet state, $(^3n\pi^*/^1\pi\pi^*)_{STC}$, and another at 4.0 eV, further along the relaxation path and near the methanamine-like CI with the ground state. The latter crossing involves directly the lowest $^3(\pi\pi^*)$ T₁ triplet state, $(^3\pi\pi^*/^1\pi\pi^*)_{STC}$, and it has a structure displaying the same type of envelope puckered geometry³⁹ with a stretched and twisted double $C_2=N_3$ bond, as at the $(gs/^1\pi\pi^*)$ CI.^{29,38} At

these two STC regions, the computed electronic SOC terms are 2 ($^3n\pi^*/^1\pi\pi^*$) and 7 cm^{-1} ($^3\pi\pi^*/^1\pi\pi^*$). These values can be considered in agreement with the qualitative El-Sayed rules, which pointed to large SOC terms for states of different natures and small otherwise.⁶² El-Sayed rules were developed for molecules near the FC region, where most of the (organic) molecules considered were planar, and their identity, $\pi\pi^*$, $n\pi^*$, etc., could be qualitatively described as such. Far from the FC region, in particular, close to a strongly distorted and puckered geometry like the ^2E CI, the same rules are not so easy to apply. For instance, the $\pi\pi^*$ state at this region, due to the out-of-plane distortion, has a close diradical character with two electrons in orbitals that are almost perpendicular to each other, the same as the $n\pi^*$ state in the FC region. This effect is particularly true for the low-energy singlet–triplet crossing region, which will be shown to be common in all nucleobases. The presence of the STCs combined with large electronic SOC terms are necessary, but not sufficient, conditions to guarantee efficient ISC processes, but they are good indications of relevant regions in which the population transfer toward the triplet states may take place, provided that the wave packet remains there for a long enough time for the ISC process to take place. The high-energy (~ 5.2 eV) $^1\pi\pi^* \rightarrow ^3n\pi^*$ STC area, not far from the FC absorption region, fulfills those conditions. On the other hand, recent reaction dynamics calculations suggest⁴⁵ that the region of the (gs/ $^1\pi\pi^*$)_{CI} (reached in femtoseconds), where also the STC takes place, represents an area in which the system stays trapped for some time (due to the structure of the CI) until the population switch toward the ground state takes place, which could also explain the slower picosecond channel observed in nucleobases.¹⁷ Figure 3 includes a scheme describing the population of T_1 based on our CASPT2 calculations.

From each one of the STC regions, we have computed corresponding MEPs along the populated triplet states, $^3(n\pi^*)$ and $^3(\pi\pi^*)$, for the suggested high- and low-energy ISC channels, respectively (they can be found in the SI). Soon, along the MEP on $^3(n\pi^*)$, a crossing with the lowest-lying $^3(\pi\pi^*)$ state takes place. The corresponding CI, ($^3n\pi^*/^3\pi\pi^*$)_{CI}, represents another funnel for efficient energy transfer within the triplet manifold. Additionally, as the singlet $^1(n\pi^*)$ state lies very close to the triplet counterpart and their PEHs run almost parallel, an STC ($^1n\pi^*/^3\pi\pi^*$) also occurs at that region. Considering that the computed SOC term in this case rises to 15 cm^{-1} , the corresponding ISC process toward the $^3(\pi\pi^*)$ state should be considered very favorable. A subsequent MEP from the ($^3n\pi^*/^3\pi\pi^*$)_{CI} along the ($^3\pi\pi^*$) PEH leads to the lowest triplet state minimum (see SI). Regarding the STC described at 4.0 eV, the MEP computed from the ($^3\pi\pi^*/^1\pi\pi^*$)_{STC} along the ($^3\pi\pi^*$) state leads directly to the minimum of the triplet state (see SI). The involvement of a dark singlet $n\pi^*$ state on adenine relaxation dynamics was previously suggested by other authors to explain slow decay features.^{17,63,64}

After the lowest triplet state is populated by any of the previous ISC processes, the system is finally expected to evolve toward the triplet state minimum, $^3(\pi\pi^*)_{\text{min}}$ (see Figure 3), which is characterized by a structure with almost planar rings but with the terminal hydrogen C₈H lifted near

40° and with an increased bond length C₂N₃ of 1.389 Å (compared to 1.311 Å in the ground state), in agreement with previous estimations.⁵⁵ The reactivity that could be attributed to this triplet state originates from its biradical character on C₂ and N₃. The minimum is placed at 3.36 eV adiabatically (see Table 1) from the ground state optimized minimum, a value consistent with the measured phosphorescence band origin in solution at 3.43,⁵⁸ and other theoretical results.^{43,55} We have also located the singlet–triplet crossing connecting the $^3(\pi\pi^*)$ and the ground state and mapped the MEP leading from such an STC toward $^3(\pi\pi^*)_{\text{min}}$ (see SI). The crossing is placed near 4.0 eV from the ground state minimum, which means that there is a barrier of near 0.6 eV (14.0 kcal/mol) to reach (gs/ $^3\pi\pi^*$)_{STC} from $^3(\pi\pi^*)_{\text{min}}$. The distortion of the five-membered ring is larger at the STC point, and the computed electronic SOC is somewhat low, ~ 2 cm^{-1} , suggesting for the triplet state a long lifetime and a slow relaxation, becoming therefore prone to reacting or transferring its energy by photosensitization mechanisms.^{8–10}

In summary, we have identified in adenine (see Figure 3) three possible intrinsic ISC channels toward the lowest triplet state which can be easily accessed from the main barrierless MEP for singlet decay dynamics, two of them mediated by $n\pi^*$ states. In all three cases, the magnitude of the computed SOC terms between the relevant states is high enough to suggest an efficient population of the triplet manifold in adenine upon UV irradiation. This type of $^1\pi\pi^*/^3\pi\pi^*$ ISC mechanism via intermediate $n\pi^*$ states can be suggested here as favorable, even far from the FC region, as it has been recently reported also for other biological chromophores such as isoalloxazine⁶⁵ and psoralen.⁶⁶ Both mechanisms described here can in any case contribute to the overall population of the lowest triplet state. In principle, in different environments, such as in polar solvents, it is expected that the $n\pi^*$ -type excited state will become destabilized with respect to $\pi\pi^*$ -type excited states.⁶⁷ Despite those effects, both singlet and triplet $n\pi^*$ -type states are estimated to lie in the solvent below the $^1(\pi\pi^* \text{ L}_a)$ state at the FC geometry,⁶⁸ guaranteeing the existence of the STC crossing upon decay along the $^1(\pi\pi^* \text{ L}_a)$ state. Intersystem crossing quantum yields have been measured by means of nanosecond laser photolysis in adenine to be 0.23×10^{-2} higher than in guanine.⁷ Likewise, phosphorescence quantum yields of 4.5×10^{-2} for adenine in frozen solutions at 77 K have been reported, slightly higher than for guanine, 3.6×10^{-2} and 2×10^{-2} ,^{69,70} and lower than thymine.⁷ For the purine nucleobases, the ISC yield has been measured to be lower in the nucleotide.⁷ Also in adenine,⁷¹ although less clearly documented as in pyrimidine nucleobases, a wavelength dependence of the intersystem crossing quantum yield in nucleobases has been reported, as it can be expected by the contribution of the three (at excitation energies higher than 5.0 eV) or just the lowest-energy (at energies close to 4.0 eV) ISC mechanisms. This point requires further experimental confirmation.

B. Population of the Triplet Manifold in Guanine. The same strategy as for adenine has been followed in the calculations of guanine. Table 2 lists the main spectroscopic properties of the lowest-lying singlet and triplet states of the

Table 2. Computed Properties for the Low-Lying Singlet and Triplet Excited States of Guanine

state	vertical transition (eV)		band origin (T _e , eV)		τ_{rad}^b
	CASSCF	CASPT2 ^a	CASSCF	CASPT2	
¹ (L _a $\pi\pi^*$) ^c	6.36	4.93 (0.158)			
¹ (n _O π^*)	5.70	5.54 (0.002)	4.04	4.56	6800 ns
¹ (L _b $\pi\pi^*$)	7.04	5.72 (0.145)	6.07	5.69	5 ns
³ (L _a $\pi\pi^*$)	3.97	4.11	3.13	3.15	3562 ms
³ ($\pi\pi^*$)	5.08	4.76			
³ ($\pi\pi^*$)	5.41	5.14			
³ (n _O π^*)	5.82	5.30	4.64	4.17	

^a Oscillator strengths within parentheses. ^b Computed using the Strickler–Berg approximation. See SI. ^c Geometry optimization leads directly to a conical intersection with the ground state, (gs/ $\pi\pi^*$)CI, at 4.3 eV. See ref.³⁹

molecule. As compared to adenine, a couple of important aspects of the electronic structure of guanine have to be highlighted. First of all is the low energy displayed by the ¹($\pi\pi^*$ L_a) HOMO → LUMO state, placed at 4.93 eV at the FC region as the lowest-energy feature. The value of the related oscillator strength, 0.158, indicates that this is the bright singlet state basically populated in the low-energy absorption spectrum, and that the relevant photophysics of the system will take place along the MEP on such a state. The second aspect is related to the high-energy of the low-lying n π^* states, which are placed near 0.6 (singlet) and 0.4 (triplet) eV above the ¹($\pi\pi^*$ L_a) state (even higher in solution). As is clear from Table 2, and also from Figure 4, the gap between the initially populated singlet state and the n π^* states is much larger than in adenine. At the FC region, it is therefore expected that an ISC process relating the ¹($\pi\pi^*$ L_a) and ³n π^* states is less favorable than for adenine.

Figure 4 displays the MEP from the FC structure and along the ¹($\pi\pi^*$ L_a) state. At the beginning of the MEP, the singlet state only crosses with the second triplet ³($\pi\pi^*$) state. The computed electronic SOC terms are small (<0.1 cm⁻¹), and only strongly coupled vibronic terms would enhance in this region the ISC rate. Near point 9 of the MEP, the singlet state crosses with the lowest triplet state, as it occurred in adenine. The STC region, placed adiabatically at 4.3 eV, is not far from the CI between the singlet and the ground state. The corresponding SOC terms are much larger here, 8 cm⁻¹, and therefore a more efficient ISC process leading directly to the population of the lowest ³($\pi\pi^*$) state can be therefore expected, or at least proposed. As compared with adenine, however, the overall population of the triplet manifold cannot be expected to be favorable. Even when the ³(n_O π^*) excited state minimum lies lower in energy than the (gs/ $\pi\pi^*$)CI, and therefore a crossing with the ¹($\pi\pi^*$) state takes place at some other region, the key point is that such a crossing cannot be easily accessed from the photochemically relevant MEP, that is, the main decay path for singlet deactivation. As a matter of fact, we have computed the STC crossing structure (³n_O π^* /¹ $\pi\pi^*$)_{STC}, which lies almost degenerate with the computed (¹n_O π^* /¹ $\pi\pi^*$)_{CI} (see ref 39), at 4.6 eV, but far from the main MEP region, because it represents the stretching and twisting of the C₆N₁ bond. Even when such a structure, in which the SOC is large enough, 8 cm⁻¹, can be accessed with excess energy, it cannot be considered as favorable as those reached via the MEP-related channels.

For the sake of completeness, we have connected the mentioned STC points with the minimum of the lowest ³($\pi\pi^*$) state by computing the corresponding MEPs: (i) from the computed (³ $\pi\pi^*$ /¹ $\pi\pi^*$)_{STC} and (³n_O π^* /¹ $\pi\pi^*$)_{STC} structures along the ³($\pi\pi^*$) and ³(n_O π^*) states, leading to their respective minima, (ii) from the computed (³n_O π^* /³ $\pi\pi^*$)_{CI} to the ³($\pi\pi^*$) minimum, and (iii) from the singlet–triplet (¹gs/³ $\pi\pi^*$)_{STC} toward the final ³($\pi\pi^*$) minimum. All them are possible paths leading to the population of the lowest triplet state, although we emphasize that, unlike adenine, only the lowest-lying 4.3 eV ISC mechanism related to the (³ $\pi\pi^*$ /¹ $\pi\pi^*$) STC should be initially considered efficient, because it is the only one taking place in the proximity of the main ¹($\pi\pi^*$ L_a) MEP (see Figure 5 for a scheme of the triplet photophysics in guanine). Finally, the ³($\pi\pi^*$) minimum has been connected through a corresponding MEP with the STC with the ground state, (gs/³ $\pi\pi^*$)_{STC}. Although the SOC terms at this point are higher than in adenine, the barrier from the minimum, placed at 3.15 eV, is too large (0.85 eV) to expect an efficient decay to the ground state. All computed MEPs can be found in the SI. At the ³($\pi\pi^*$) minimum, the molecule displays a slightly puckered envelope structure on the six-membered ring,³⁹ with the C₂N₃ bond having a biradical character and enlarged up to 1.438 Å, as compared to 1.286 Å at the FC ground-state geometry.

It has to be finally mentioned that guanine is the only natural nucleobase in which no phosphorescence data or triplet state formation has been reported for the parent compound, although intersystem crossing⁷ and phosphorescence quantum yields of 0.042 and 0.095 have been reported for the nucleoside and nucleotide in ethanol,⁶ 5 to 7 times larger than the fluorescence quantum yields. It has to be remembered also that the natural keto form of 9H-guanine is not the most stable in the gas phase and that other close tautomers can contribute to the measurements for the isolated system,^{39,72} not in an oligomer sample.

C. Population of the Triplet Manifold in Pyrimidine Nucleobases: Thymine, Uracil, and Cytosine. For the sake of brevity, we will discuss the triplet manifold population of the pyrimidine nucleobases together within the same framework. The computational strategies followed have been those described above for adenine and guanine. As uracil has a state structure and triplet photophysics very similar to that of thymine, we will refer to our previous results²⁵ and concentrate on the latter. Thymine has, at the FC region, a low-lying ¹(n_O π^*) state (basically related to the O₄ atom), placed 0.2 eV below the spectroscopic ¹($\pi\pi^*$ L_a) HOMO → LUMO state, this one lying at 4.89 eV with a related oscillator strength of 0.167 (see Table 3). The photophysical mechanisms proposed for the population of the lowest triplet state will be very similar to those already explained for adenine, as Table 3 and Figures 6 and 7 can confirm. Once more, the key point is that three different STC regions can be easily accessed through the main decay path of the energy, as it is the FC ¹($\pi\pi^*$ L_a) MEP, being prospective channels for ISC toward the lowest-lying triplet state.

Soon after the beginning of the MEP (see Figure 6), the ¹($\pi\pi^*$ L_a) state crosses with both singlet and triplet n π^* states. Apart from a possible IC toward the singlet ¹(n_O π^*)

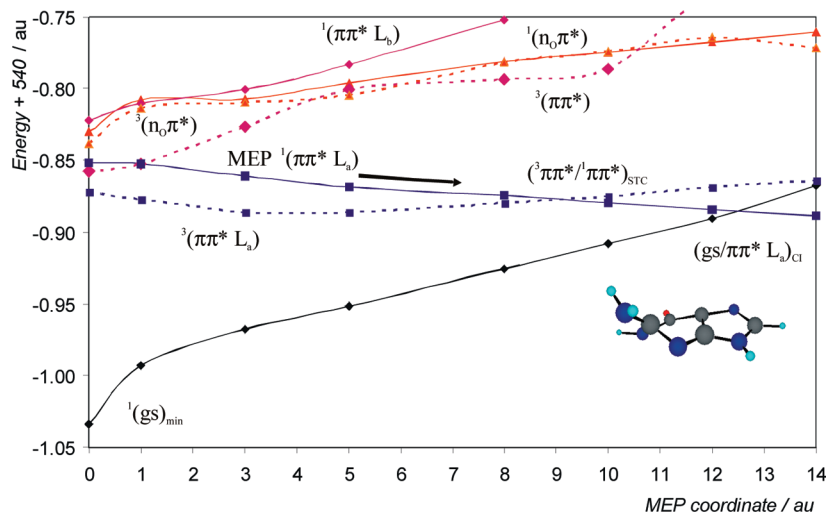


Figure 4. Evolution of the ground and lowest singlet and triplet excited states for guanine from the FC geometry along the $^1(\pi\pi^* L_a)$ MEP.

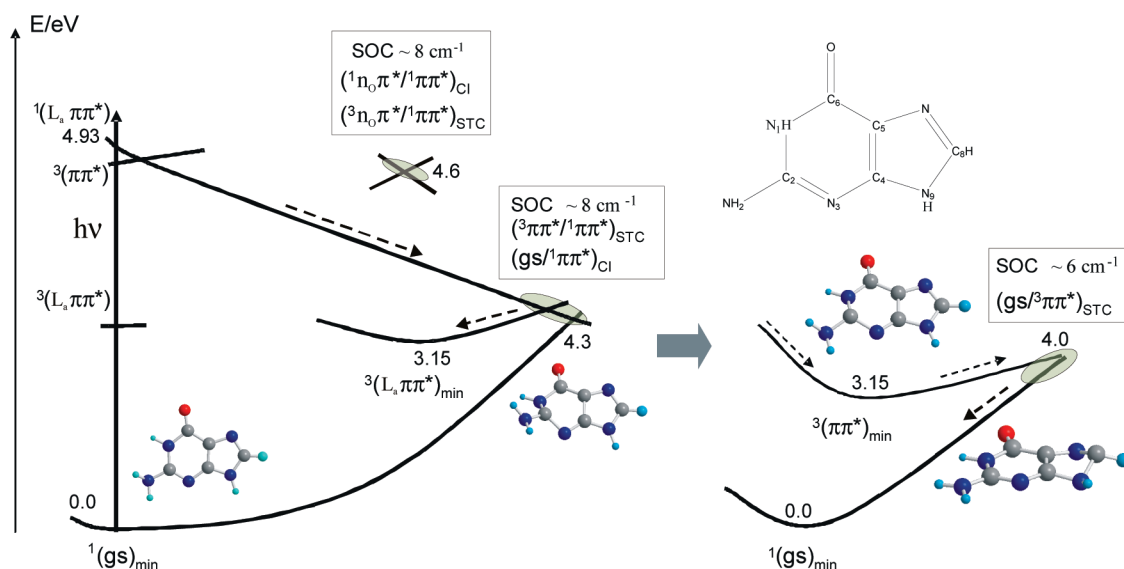


Figure 5. Scheme, based on CASPT2 results, of the photochemistry of guanine focused on the population of the lowest-energy triplet state. Unless otherwise stated, $^1\pi\pi^*$ represents the $^1L_a \pi\pi^*$ state.

Table 3. Computed Properties for the Low-Lying Singlet and Triplet Excited States of Thymine^a

state	vertical transition (eV)		band origin (T_e , eV)		
	CASSCF	CASPT2 ^b	CASSCF	CASPT2	τ_{rad}^c
$^1(n_O\pi^*)^d$	5.41	4.77 (0.004)	4.23	4.05	2501 ns
$^1(\pi\pi^* L_a)$	6.52	4.89 (0.167)	6.07	4.49	9 ns
$^1(\pi\pi^*)$	7.36	5.94 (0.114)			
$^3(\pi\pi^* L_a)$	3.95	3.59	2.99	2.87	17 ms
$^3(n_O\pi^*)^d$	5.21	4.75	3.84	3.93	
$^3(\pi\pi^*)$	5.86	5.14			

^a See also ref 24. ^b Oscillator strengths within parentheses.

^c Computed using the Strickler–Berg approximation. See SI.

^d Involving basically O_4 (in ortho position with methyl group).

state through a corresponding CI, this region may be responsible for the first ISC process taking place in thymine at high energies (4.8 eV), in which the $^3(n_O\pi^*)$ state could be populated from the initially activated singlet $\pi\pi^*$ state. The SOC terms, computed as 8 cm^{-1} , point to the efficiency of the process. Another MEP computed from this crossing and along the $^3(n_O\pi^*)$ PEH leads the system toward the

minimum of this state, in whose neighborhood we have found the conical intersection with the lowest triplet state, $(^3n_O\pi^*/^3\pi\pi^*)_{\text{CI}}$, near 3.9 eV. As the singlet and triplet $n\pi^*$ PEHs are always very close along the MEP, near the CI we have also found the $(^1n_O\pi^*/^3\pi\pi^*)_{\text{STC}}$. In case some population reaches the $^1(n_O\pi^*)$ state via the higher-energy crossing with $^1(\pi\pi^* L_a)$ —and a decay path through this dark intermediate has been recently reported⁶⁸—the energy switch toward the lowest triplet state would be extremely favorable, because the computed SOC term increases in the $(^1n_O\pi^*/^3\pi\pi^*)_{\text{STC}}$ region to 61 cm^{-1} . It is possible to confirm our suggestions about the effectiveness of this type of mechanism thanks to the recent study by Etinski et al.,²⁶ which has established the efficiency of the $(^1n_O\pi^*/^3\pi\pi^*)_{\text{STC}}$ ISC channel by computing vibrational FC factors and ISC rates. Either by triplet–triplet IC or by singlet–triplet ISC, the final population process of the lowest $^3(\pi\pi^*)$ state should be considered to be extremely favorable. As in the other nucleobases, a low-energy STC region lies close to the end of the FC $^1(\pi\pi^*)$

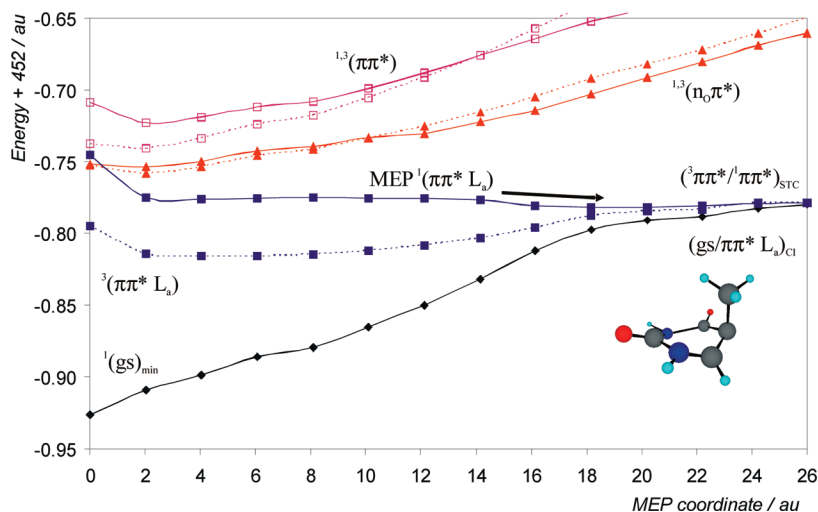


Figure 6. Evolution of the ground and lowest singlet excited states for thymine from the FC geometry along the $^1(\pi\pi^* L_a)$ MEP.

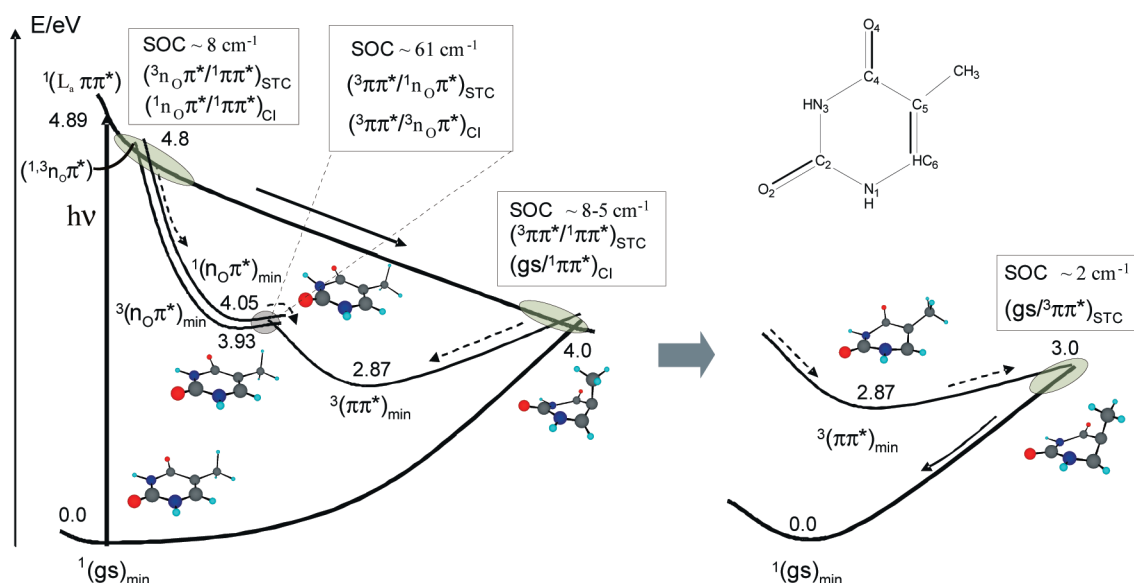


Figure 7. Scheme, based on CASPT2 results, of the photochemistry of thymine focused on the population of the lowest-energy triplet state. Unless otherwise stated, $^1\pi\pi^*$ represents the $^1L_a \pi\pi^*$ state.

L_a MEP, at 4.0 eV. As observed in Figure 6, this area of the PEH is flat and extended close to the end of the MEP. The SOC values computed at different points along the path range from 5 to 8 cm^{-1} . The efficiency of the process would be also high if, as in adenine, the wave packet decaying through the singlet manifold is delayed in the region of the singlet–singlet CI. The present model allows for an understanding of the reported wavelength dependence on the ISC quantum yield in nucleobases, surely caused by the location of the two STC interacting regions and their accessibility upon the initial excitation conditions. In the case of thymine, the value increases from 3.9×10^{-3} at 280 nm (4.43 eV), where only the lowest-energy channel can be reached, to 5.2×10^{-2} at 240 nm (5.17 eV),^{7,73} where both described channels are accessible.

As for the purine nucleobases, MEPs connecting the different critical points have been computed (see SI). The lowest triplet state may be populated by any of the previous ISC processes. At the state minimum, the molecule displays

a distorted structure with a ring deformation including the dihedral angle $C_2N_1C_6C_5$ as 44° and an increased bond length C_5C_6 of 1.494 \AA with certain biradical character. The minimum is placed at 2.87 eV adiabatically from the ground state optimized minimum, a value somewhat lower than the 3.2 eV estimated for the location of the triplet state for the thymine mononucleotide in aqueous solution at room temperature⁹ and consistent with previous theoretical determinations at around 2.8–3.0 eV.⁷⁴ As a final aspect of the evolution along the triplet manifold in thymine, we have located the singlet–triplet crossing connecting the $^3(\pi\pi^*)$ and the ground state and mapped the MEP leading from such an STC toward $^3(\pi\pi^*)_{\min}$ (see SI). The crossing is placed near 3.0 eV from the ground state minimum, which means that there is a barrier of 0.13 eV (3.0 kcal/mol) to reach $(gs/{}^3\pi\pi^*)_{\text{STC}}$ from $^3(\pi\pi^*)_{\min}$, and the molecule recovers there the planarity. Although the computed electronic SOC is somewhat low, $\sim 2\text{ cm}^{-1}$, a barrier which is smaller than that for purines may explain the shorter triplet lifetimes

Table 4. Computed Properties for the Low-Lying Singlet and Triplet Excited States of Cytosine

state	vertical transition (eV)		band origin (T_e , eV)		τ_{rad}^b
	CASSCF	CASPT2 ^a	CASSCF	CASPT2	
¹ (L _a $\pi\pi^*$) ^c	5.22	4.41 (0.069)	4.14	3.62	30 ns
¹ (nO π^*)	5.23	4.95 (0.001)	3.68	3.72	1200 ns
¹ (nN π^*) ^d	5.59	5.06 (0.003)			
¹ (L _b $\pi\pi^*$)	6.17	5.89 (0.106)			
³ (L _a $\pi\pi^*$)	3.64	3.53	2.85	2.98	437 ms
³ ($\pi\pi^*$)	4.87	4.45			
³ (nO π^*)	5.13	4.63	3.49	3.66	
³ (nN π^*)	5.31	4.94			

^a Oscillator strengths within parentheses. ^b Computed using the Strickler–Berg approximation. See SI. ^c The MEP to the minimum and the CI, (gs/ $\pi\pi^*$)_{CI}, at 3.6 eV, are competitive. See ref 37. ^d Geometry optimization leads directly to a CI with the ground state, (gs/nN π^*)_{CI}. See ref 76.

measured for pyrimidine (~ 0.6 s) than for purine (~ 2.0 s) nucleobases in ethanol glasses.⁶ Similar conclusions can be derived for uracil, which has a state structure and properties very similar to those of thymine.^{25,26}

Regarding cytosine, the values in Table 4 help to understand (and predict to some extent) the behavior of its triplet photophysics. As in guanine, cytosine has a lowest-lying singlet ¹($\pi\pi^*$ L_a) state, whose initial interaction with the n π^* states, placed higher in energy, will not be strong either at the FC region or along the ¹($\pi\pi^*$ L_a) decay pathway (see Figure 8). The singlet relaxation in C is somewhat more complex than in the other nucleobases. The presence of a low-lying planar minimum for the ¹($\pi\pi^*$ L_a) state at 3.62 eV, nearly isoenergetic with the ethene-like (gs/ $\pi\pi^*$)_{CI}, generates several competitive decay paths, as has been analyzed before.^{23,37,75} The possibilities for displaying different ISC processes are therefore larger, but always at low, not at high, energies like, for instance, in thymine, uracil, or adenine. In particular, we show in Figure 8 a linear interpolation in internal coordinates (LIIC) path from the FC region toward the ethene-like CI with the ground state. The barrier along the ¹($\pi\pi^*$ L_a) state, computed 2.5 kcal mol^{−1} as a higher bound, is very small, and in practice the path can be considered barrierless. As in the other nucleobases, an STC between the lowest $\pi\pi^*$ states takes place close to the CI, at 3.6 eV, yielding a SOC term value of 6 cm^{−1}. In a previous study,²³ we analyzed ISC processes taking place at other low-energy regions, obtaining also large SOC values and expectedly favorable situations for the lowest triplet population.

As a result of the excited state structure in C, obtained at the CASPT2 level, the photophysical scheme for the population of the lowest triplet state of the molecule can be summarized in Figure 9. Unlike in the other two pyrimidine nucleobases, where three basic channels for the possible triplet manifold population were found, one at high energies (close to FC and n π^* mediated) and another at low energies (caused by the common ethene-like CI type of decay present in all nucleobases), in C, only low-energy channels seem to be accessible. This feature could probably help to explain the absence of cytosine (guanine too) components in DNA phosphorescence at low temperatures,^{1–3} and also the generally lower phosphorescence quantum yields obtained for cytosine and its derivatives as compared to other

nucleobases.⁶ The same trends are obtained for ISC yields from flash photolysis experiments in nucleotides, although not in nucleobases.⁷ Higher yields of n π^* formation have been suggested for cytosine than thymine,⁶⁸ but theoretical evidence indicates that the higher-lying n π^* states of cytosine will be less accessible from the main relaxation pathways than in thymine due to the large potential energy barriers found in the former.⁷⁶

IV. Summary and Conclusions

Calculation of PEHs for the low-lying singlet and triplet states of natural DNA/RNA nucleobases adenine, guanine, thymine, uracil, and cytosine at the *ab initio* multiconfigurational CASPT2//CASSCF quantum-chemical level have been carried out in order to help to establish general mechanisms for the population of the triplet manifold of the molecules. The proposed framework is an attempt to rationalize the reported triplet states properties of DNA components, in particular the measurement of larger quantum yields of phosphorescence than of fluorescence in the individual systems,^{4,7} the observed wavelength dependence of the triplet state formation,^{7,73} or the prevalence of adenine and thymine components in the phosphorescence signals of DNA at low temperatures.^{1–3} It can be considered that an efficient ISC channel is easily accessible from the regions close to the main decay pathway of the initially populated singlet state. We have analyzed the accessibility of the ISC channels for the population of the lowest triplet state along such a pathway, a strategy that requires computation of minimum energy paths on the different states and determination of singlet–triplet crossings and conical intersections. This is, however, only a necessary but not sufficient condition to establish the efficiency of an ISC process. Computation of vibronic contributions to the ISC rates and reaction dynamic calculations establishing the temporal evolution of the system are encouraged in a close future in order to unambiguously determine if the proposed accessible singlet–triplet crossing regions fulfill all the requirements: close singlet–triplet energies, a high density of vibronic states, large vibronic contributions to the spin–orbit coupling terms, and regions where the population gets trapped for long enough of a time to allow the ISC process to take place in competition with the internal conversion decay, for instance, close to the FC region, to a singlet state minimum, or near a sloped conical intersection. Recent ISC rate calculations on thymine and uracil²⁶ confirm the main role of some of our proposed ISC mechanisms in these systems.

Our results indicate that three STC regions can be easily accessed from the singlet main decay pathway in adenine, thymine, and uracil, two of them located at high energies and mediated by the presence of lowest-lying singlet and triplet n π^* states, and a third one at low energies close to the end of the main MEP on the ¹($\pi\pi^*$) singlet excited state and the ethene-like (pyrimidines) or methanamine-like (purines) conical intersection of this state with the ground state. These three regions are proposed as prospective ISC channels. At least those related to the ¹n π^* –³ $\pi\pi^*$ STC seem to be confirmed as such by recent calculations on ISC rates on pyrimidine nucleobases.²⁶ Additionally, the wavelength

of the singular points. This material is available free of charge via the Internet at <http://pubs.acs.org>.

References

- (1) Imakubo, K. *J. Phys. Soc. Jpn.* **1968**, *24*, 1124.
- (2) Szerenyi, P.; Dearman, H. H. *Chem. Phys. Lett.* **1972**, *15*, 81.
- (3) Arce, R.; Rodríguez, G. *J. Photochem.* **1986**, *33*, 89.
- (4) Gueron, M.; Eisinger, J.; Lamola, A. A. Excited States of Nucleic Acids. In *Basic Principles in Nucleic Acid Chemistry*; Tso, P. O. P., Ed.; Academic Press: New York, 1974; Vol. 1, pp 311–398.
- (5) Daniels, M. In *Photochemistry and Photobiology of Nucleic Acids*; Wang, S. Y., Ed.; Academic Press: New York, 1976; Vol. 1, pp 23–108.
- (6) Görner, H. *J. Photochem. Photobiol. B: Biol.* **1990**, *5*, 359.
- (7) Cadet, J.; Vigny, P. In *Bioorganic Photochemistry*; Morrison, H., Ed.; John Wiley & Sons: New York, 1990; Vol. 1, pp 1–272.
- (8) Gut, I. G.; Wood, P. D.; Redmond, R. W. *J. Am. Chem. Soc.* **1996**, *118*, 2366.
- (9) Wood, P. D.; Redmond, R. W. *J. Am. Chem. Soc.* **1996**, *118*, 4256.
- (10) Bosca, F.; Lhiaubet-Vallet, V.; Cuquerella, M. C.; Castell, J. V.; Miranda, M. A. *J. Am. Chem. Soc.* **2006**, *128*, 6318.
- (11) Kang, H.; Lee, K. T.; Jung, B.; Ko, Y. J.; Kim, S. K. *J. Am. Chem. Soc.* **2002**, *124*, 12958–12959.
- (12) Klessinger, M. In *Theoretical Organic Chemistry - Theoretical and Computational Chemistry*; Párkányi, C., Ed.; Elsevier: Amsterdam, 1998; p 581.
- (13) Serrano-Pérez, J. J.; Merchán, M.; Serrano-Andrés, L. *J. Phys. Chem. B.* **2008**, *112*, 14002.
- (14) Brown, I. H.; Johns, H. E. *Photochem. Photobiol.* **1968**, *8*, 273.
- (15) Schreier, W. J.; Schrader, T. E.; Koller, F. O.; Gilch, P.; Crespo-Hernández, C. E.; Swaminathan, V. N.; Carell, T.; Zinth, W.; Kohler, B. *Science* **2007**, *315*, 625.
- (16) Roca-Sanjuán, D.; Olaso-González, G.; González-Ramírez, I.; Serrano-Andrés, L.; Merchán, M. *J. Am. Chem. Soc.* **2008**, *130*, 10768.
- (17) Crespo-Hernández, C. E.; Cohen, B.; Hare, P. M.; Kohler, B. *Chem. Rev.* **2004**, *104*, 1977–2019.
- (18) Serrano-Andrés, L.; Merchán, M. In *Radiation Induced Molecular Phenomena in Nucleic Acid: A Comprehensive Theoretical and Experimental Analysis*; Shukla, M. K., Leszczynski, J., Eds.; Springer: The Netherlands, 2008; pp 435–472.
- (19) Middleton, C. T.; De La Harpe, K.; Su, C.; Law, Y. K.; Crespo-Hernández, C. E.; Kohler, B. *Annu. Rev. Phys. Chem.* **2009**, *60*, 217.
- (20) Serrano-Andrés, L.; Merchán, M. *J. Photochem. Photobiol. C: Photochem. Rev.* **2009**, *10*, 21.
- (21) Conti, I.; Garavelli, M.; Orlandi, G. *J. Am. Chem. Soc.* **2009**, *131*, 16108.
- (22) Conti, I.; Altoè, P.; Stenta, M.; Garavelli, M.; Orlandi, G. *Phys. Chem. Chem. Phys.* **2010**, DOI: 10.1039/b926608a (accessed May 4, 2010).
- (23) Merchán, M.; Serrano-Andrés, L.; Robb, M. A.; Blancafort, L. *J. Am. Chem. Soc.* **2005**, *127*, 1820.
- (24) Serrano-Pérez, J. J.; González-Luque, R.; Merchán, M.; Serrano-Andrés, L. *J. Phys. Chem. B.* **2007**, *111*, 11880.
- (25) Climent, T.; González-Luque, R.; Merchán, M.; Serrano-Andrés, L. *Chem. Phys. Lett.* **2007**, *441*, 327.
- (26) Etinski, M.; Fleig, T.; Marian, C. M. *J. Phys. Chem. A* **2009**, *113*, 11809.
- (27) Klessinger, M.; Michl, J. *Excited States and Photochemistry of Organic Molecules*; VCH Publishers, Inc.: New York, 1995.
- (28) *Computational Photochemistry*; Olivucci, Ed.; Elsevier: Amsterdam, 2005.
- (29) Serrano-Andrés, L.; Merchán, M.; Borin, A. C. *Proc. Natl. Acad. Sci. U.S.A.* **2006**, *103*, 8691.
- (30) Tatchen, J.; Gilka, N.; Marian, C. M. *Phys. Chem. Chem. Phys.* **2007**, *9*, 5209.
- (31) Salzmann, S.; Tatchen, J.; Marian, C. M. *J. Photochem. Photobiol. A* **2008**, *198*, 221.
- (32) Carpenter, B. K. *Chem. Soc. Rev.* **2006**, *35*, 736.
- (33) Harvey, J. N.; Poli, R.; Smith, K. M. *Coord. Chem. Rev.* **2003**, *238–239*, 347.
- (34) González-Navarrete, P.; Coto, P. B.; Polo, V.; Andrés, J. *Phys. Chem. Chem. Phys.* **2009**, *11*, 7189.
- (35) Atchity, G. J.; Xantheas, S. S.; Ruedenberg, K. *J. Chem. Phys.* **1991**, *95*, 1862.
- (36) Ben-Nun, M.; Molnar, F.; Schulten, K.; Martinez, T. J. *Proc. Natl. Acad. Sci. U.S.A.* **2002**, *99*, 1769.
- (37) Merchán, M.; González-Luque, R.; Climent, T.; Serrano-Andrés, L.; Rodríguez, E.; Reguero, M.; Peláez, D. *J. Phys. Chem. B* **2006**, *110*, 26471.
- (38) Serrano-Andrés, L.; Merchán, M.; Borin, A. C. *Chem.—Eur. J.* **2006**, *12*, 6559.
- (39) Serrano-Andrés, L.; Merchán, M.; Borin, A. C. *J. Am. Chem. Soc.* **2008**, *130*, 2473.
- (40) Blancafort, L. *J. Am. Chem. Soc.* **2006**, *128*, 210.
- (41) Perun, S.; Sobolewski, A. L.; Domcke, W. *J. Am. Chem. Soc.* **2005**, *127*, 6257.
- (42) Perun, S.; Sobolewski, A. L.; Domcke, W. *J. Phys. Chem. A* **2006**, *110*, 13238.
- (43) Marian, C. M. *J. Chem. Phys.* **2005**, *122*, 104314.
- (44) Chen, H.; Li, S. H. *J. Phys. Chem. A* **2005**, *109*, 8443.
- (45) Barbatti, M.; Lischka, H. *J. Am. Chem. Soc.* **2008**, *130*, 6831.
- (46) Hudock, H. R.; Martinez, T. J. *ChemPhysChem* **2008**, *9*, 2486.
- (47) Canuel, C.; Mons, M.; Pluzzi, F.; Tardivel, B.; Dimicoli, I.; Elhanine, M. *J. Chem. Phys.* **2005**, *122*, 074316.
- (48) Bernardi, F.; Olivucci, M.; Robb, M. A. *Pure Appl. Chem.* **1995**, *67*, 17.
- (49) Takaya, T.; Su, C.; De La Harpe, K.; Crespo-Hernández, C. E.; Kohler, B. *Proc. Natl. Acad. Sci. U.S.A.* **2008**, *105*, 10285.
- (50) Olaso-González, G.; Merchán, M.; Serrano-Andrés, L. *J. Am. Chem. Soc.* **2009**, *131*, 4368.
- (51) Strickler, S. J.; Berg, R. A. *J. Chem. Phys.* **1962**, *37*, 814.
- (52) Rubio-Pons, O.; Serrano-Andrés, L.; Merchán, M. *J. Phys. Chem. A* **2001**, *105*, 9664.

- (53) Veryazov, V.; Widmark, P.-O.; Serrano-Andrés, L.; Lindh, R.; Roos, B. O. *Int. J. Quantum Chem.* **2004**, *100*, 626.
- (54) Aquilante, F.; De Vico, L.; Ferré, N.; Ghigo, G.; Malmqvist, P.-Å.; Pedersen, T.; Pitonak, M.; Reiher, M.; Roos, B. O.; Serrano-Andrés, L.; Urban, M.; Veryazov, V.; Lindh, R. *J. Comput. Chem.* **2010**, *31*, 224.
- (55) Noguera, M.; Blancafort, L.; Sodupe, M.; Bertran, J. *Mol. Phys.* **2006**, *104*, 925.
- (56) Fleig, T.; Knecht, S.; Hättig, C. *J. Phys. Chem. A* **2007**, *111*, 5482.
- (57) Zgierski, M. Z.; Patchkovskii, S.; Lim, E. C. *Can. J. Chem.* **2007**, *85*, 124.
- (58) Cohen, B. J.; Goodman, L. *J. Am. Chem. Soc.* **1965**, *87*, 5487.
- (59) Lavík, J.; Jelínek, O.; Plášek, J. *Photochem. Photobiol.* **1979**, *29*, 491.
- (60) Sobolewski, A. L.; Domcke, W. *Phys. Chem. Chem. Phys.* **2004**, *6*, 2763.
- (61) Fülischer, M. P.; Serrano-Andrés, L.; Roos, B. O. *J. Am. Chem. Soc.* **1997**, *119*, 6168.
- (62) Lower, S. K.; El-Sayed, M. A. *Chem. Rev.* **1966**, *66*, 199.
- (63) Ullrich, S.; Schultz, T.; Zgierski, M. Z.; Stolow, A. *J. Am. Chem. Soc.* **2004**, *126*, 2262.
- (64) Ullrich, S.; Schultz, T.; Zgierski, M. Z.; Stolow, A. *Phys. Chem. Chem. Phys.* **2004**, *6*, 2796.
- (65) Climent, T.; González-Luque, R.; Merchán, M.; Serrano-Andrés, L. *J. Phys. Chem. A* **2006**, *110*, 13584.
- (66) Serrano-Pérez, J. J.; Merchán, M.; Serrano-Andrés, L. *Chem. Phys. Lett.* **2007**, *434*, 107.
- (67) Gustavsson, T.; Bányász, A.; Lazzarotto, E.; Markovitsi, D.; Scalamani, G.; Frisch, M. J.; Barone, V.; Improta, R. *J. Am. Chem. Soc.* **2006**, *128*, 607.
- (68) Hare, P. M.; Crespo-Hernández, C. E.; Kohler, B. *Proc. Natl. Acad. Sci. U.S.A.* **2007**, *104*, 435.
- (69) Barenboim, G. M.; Domanskii, A. N. *Luminescence of biopolymers and cells*; Plenum Press: New York, 1969; p 85.
- (70) Snipes, W. *Electron spin resonance and the effects of radiation on biological systems*; National Academy of Sciences: Washington, DC, 1966, p55.
- (71) Gupron, M.; Shulman, R. G.; Eisinger, J. *Proc. Natl. Acad. Sci. U.S.A.* **1966**, *56*, 814.
- (72) Marian, C. M. *J. Phys. Chem. A* **2007**, *111*, 1545.
- (73) Nikogosyan, D. N.; Letokhov, L. S. *Riv. Nuov. Cim.* **1983**, *6*, 1.
- (74) Nguyen, M. T.; Zhang, R.; Nam, P.-C.; Ceulemans, A. *J. Phys. Chem. A* **2004**, *108*, 6554.
- (75) Blancafort, L. *Photochem. Photobiol.* **2007**, *83*, 603.
- (76) Merchán, M.; Serrano-Andrés, L. *J. Am. Chem. Soc.* **2003**, *125*, 8108.
- (77) Kudrya, V. Y.; Yashchuk, V. M.; Levchenko, S. M.; Melnik, V. I.; Zaika, L. A.; Govorun, D. M. *Mol. Cryst. Liq. Cryst.* **2008**, *497*, 425.

CT100164M